Global Science Publishing

JITP

Journal of Information, Technology and Policy
https://ojs.sgsci.org/journals/jitp

Article

Star Map Recognition and Matching Based on Deep Triangle Model

Meng Wang [1], Huitao Zhang [2,*] and Ning Zhou [3]

[1] *Newmark Group Inc. New York, NY, USA; wang070210@gmail.com*
[2] *Northen Arizona University, Flagstaff, AZ 86011, USA*
[3] *Zhejiang Future Technology LLC, Jiaxing, China; zhouning723@gmail.com*

Abstract: The star sensor is the key component of Celestial Navigation. It measures the autonomous attitude of navigation bodies by observing stars. And it conducts image collection, preprocessing, feature extraction and matching recognition. Aimed to implement the latter two procedures, we first estimate the coordinate of the point which is the intersection point of the optical axis and the celestial sphere. We employ geometrical knowledge to get the relationship between the intersection point and given projection distances. When distances are unknown, we use Newton's method to approach the exact coordinate of the intersection point. Based on our coordinate calculation method, we are required to find a principle for improving the accuracy of the coordinate. We first establish a projection screening model to obtain star maps. Then we establish four coordinate systems, i. e., the celestial coordinate system, the star sensor coordinate system, the image coordinate system and the pixel coordinate system. Taking the star map at the north celestial pole as an instance, we finish the transformation of coordinate between different systems and search for the factors affecting accuracy of coordinate. Ultimately, we draw the conclusion that the coordinate accuracy improves, when selected stars projection close the centroid of the photosensitive surface. Aimed to implement the matching recognition, we establish a novel feature extraction and matching model. We take the angle between stars and three of their nearest stars as the feature of the central star. Then we extract the feature matrix of the given star table as the feature database. Using the same way, we get the feature matrix of four–star maps. To achieve the last step of matching recognition, we compare the feature matrix of star maps with the given navigation stars. During the process, we employ DBScan clustering algorithm to implement the matching recognition process. We select the cluster center that satisfies the maximum number of matches as the actual location of the identified star map.

Keywords: star map recognition; feature extraction; transformation of coordinate system; computer vision

1. Introduction

Celestial navigation, critical for precise spacecraft orientation, relies heavily on the capabilities of star sensors. These devices process stellar images to determine orientation, with their effectiveness significantly bolstered by advancements in computational methods, especially deep learning, as evidenced by recent work on dynamic network rewiring in deep neural networks by Kundu et al [1]. Our study advances the field of star map recognition and matching by fusing deep learning with geometric modeling, inspired by contemporary successes

Received: 8 April 2024; Accepted: 29 April 2024.

* Corresponding: Huitao Zhang (hz345@nau.edu)

in depth estimation and image processing.

Deep learning has made significant strides in a variety of fields, including recommendation systems, credit assessment, and photometric analysis [2–8]. Machine learning technology has extensive potential applications, capable of effective model prediction across various fields [9,10], and demonstrates unique applicability in the study of emotional analysis [11]. Similarly, research across various disciplines has demonstrated the significant contributions of deep learning in process optimization [12,13]. The research into advanced algorithms across various fields has demonstrated their effectiveness in enhancing efficiency and reducing costs within complex systems [14–16]. Incorporating enhanced depth estimation methods has proven pivotal in refining the accuracy of image–based navigation systems. Similarly, Deng et al.'s study on frequency–tunable plasmonic structures highlights how precise frequency control enhances sensor technologies, crucial for tackling celestial navigation challenges [17,18]. Research in extending the resolution of lidar systems through single–image depth fusion offers valuable parallels to the depth estimation challenges faced in celestial navigation [19–23]. Similarly, methodologies that enhance semantic scene understanding using normalized device coordinates provide a robust framework applicable to the spatial complexity of star maps [24–26].

The role of feature manipulation in machine learning cannot be overstated, particularly in its application to precise image analysis and recognition tasks. Techniques developed for medical image classification and change detection in dynamic scenes highlight the potential for similar strategies in star sensor data processing, enhancing the reliability of feature extraction and matching [27–32].

Advancements in computational models that integrate machine learning algorithms have also shown great promise. Notably, techniques such as those developed by Sun et al. for automatic cell activation in cloud RANs, illustrate the potential of innovative approaches in complex network settings [33]. Additionally, the application of ensemble learning techniques and vision transformers to tasks requiring high accuracy and efficiency exemplifies the types of computational strategies that can be adapted for matching recognition in star maps [34–36].

Moreover, the adaptation of sophisticated algorithms for real–time decision–making and spatial data interpretation in complex environments, such as particle filter localization and value factorization in multi–agent systems, provides a strong methodological foundation for our approach to star map recognition [37–41]. The development of graphene–based mid–infrared photodetectors is also pushing the boundaries of sensing technology [42,43].

Our proposed deep triangle model utilizes the DBScan clustering algorithm to achieve efficient and precise matching recognition [44,45]. This approach is informed by a broad spectrum of recent research across various domains, ensuring that our model not only addresses the specific challenges of celestial navigation but also aligns with the latest in scientific and computational advancements.

Determining celestial navigation parameters plays a significant role in the aerospace technology. The star sensor in Celestial Navigation technique is the key part of autonomous attitude measurement. The functions of it are image acquisition and preprocessing, feature extraction, and matching recognition. And it observes the star to attain images. After preprocessing and feature extraction, images are compared with the known star catalog, which records some positions of stars, to accomplish the last step. During the process, the celestial coordinate system, the star sensor coordinate and the image coordinate system are established to describe the location for a star.

Based on the celestial coordinate system, given positions of three stars, we are required to establish a model to calculate the coordinate of the intersection point of the optical axis and the celestial sphere. Then we need to consider how to select stars to improve the accuracy of the intersection position information if there are more than three stars in the field of view of the star sensor. In addition, we should establish a model to extract the feature for matching recognition better than traditional methods.

To solve these problems, we will process as follows:

1) Establish a tetrahedral model to compute the coordinate of the intersection point of the optical axis and the celestial sphere.

2) Compare the accuracy of the intersection point of the optical axis and the celestial sphere based on

different selection of stars.

3) After determining the principles, we extract the feature vectors of the given star tables and the star map. We use the DBScan clustering algorithm to implement the matching recognition process.

In our model, we first establish a geometrical model to compute the coordinate of the intersection point. Considering it is difficult to solve directly, we use Newton's method to simplify the equation set. Based on the first model, we get the deviation between the exact coordinate and the value we calculate. Then we use the deviation to assess the accuracy performance of selected stars. Ultimately, the principle can be concluded with the relative graph. Then we extract feature matrix of given star tables and the star table. Then we employ the matching recognition and DBScan clustering algorithm to select the best matching navigation stars.

2. Coordinate Systems, Notations and Assumptions

2.1. Establishment of Coordinate Systems

Apart from the celestial coordinate system, the star sensor coordinates system and the image coordinate system, we establish the pixel coordinate system. To get a better understanding of the questions and solutions, all establishment are described as follow.

To establish the celestial coordinate system, we need to prepare some astronomy knowledge, and all points, lines and planes are shown in Figure 1.

- The celestial sphere is an imaginary sphere of infinite radius centered on the center of the earth.
- The great circle of the celestial sphere passing through the celestial pole is called the hour circle.
- The line PP' paralleled to the earth's axis of autorotation and passing the center of the celestial sphere is named the celestial axis.
- The plane QEQ' that passes through the center of the celestial sphere and is perpendicular to the celestial axis is called the celestial equatorial plane. The intersecting circle of this plane and the celestial sphere is called the celestial equatorial.
- The average plane SEN of the earth's orbit around the sun is called the ecliptic plane. This plane intersects the celestial sphere with the ecliptic.
- The equator and the ecliptic meet at two points, one of which is named vernal equinox γ.

Taking the celestial equatorial as the base circle, the hour circle passing the spring equinox as the main circle and the spring equinox as the main point, the system defines right ascension α and declination δ to describe the location.

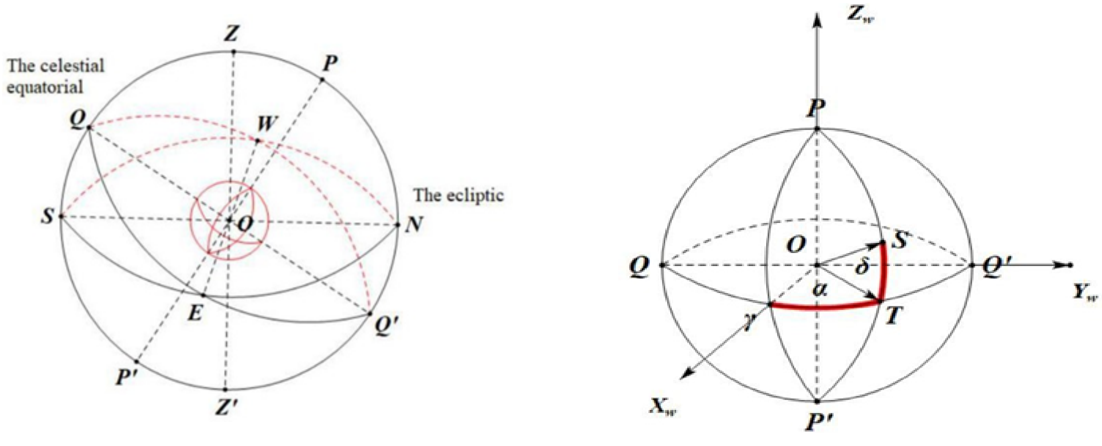

(a) **(b)**

Figure 1. The celestial coordinate system.

Then we establish the star sensor coordinate system and the image coordinate system. Set the projection center O as the origin of the star sensor coordinate system and the optical axis OD as Z_C axis, which intersect the photosensitive surface at the intersection point O'. Passing the point O,we get parallel lines of AB and BC as the X_C axis and the Y_C axis for the star sensor coordinate system. By the same way, we obtain the x axis and the y axis for the star sensor coordinate system. And the graph of systems is shown in Figure 2, the former system is the three-dimensional system and the later one is the two-dimensional system in the star sensor plane.

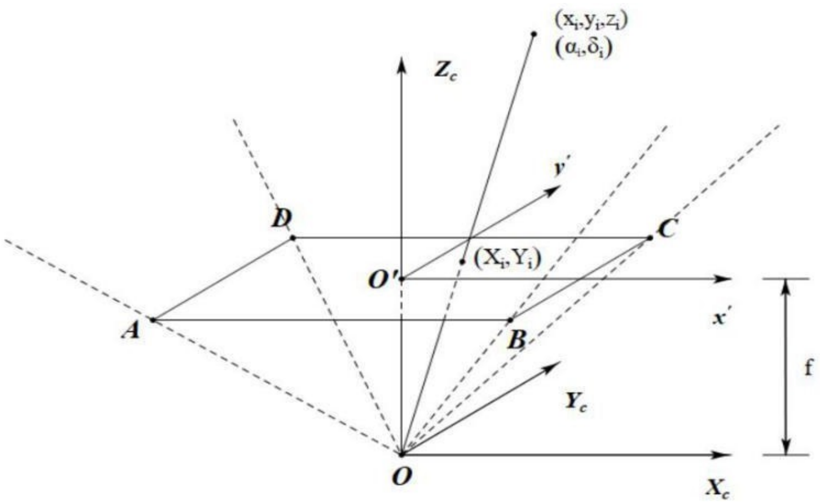

Figure 2. The star sensor coordinate system and the image coordinate system.

In addition, looking up for relevant information, we know that the field of view of the star sensor is $12^{\circ} \times 12^{\circ}$, and the pixel is 512×512. With this information, the pixel coordinate system can be established in Figure 3. Set the point A as the origin and set line AD and line AB as u–axis and v–axis respectively.

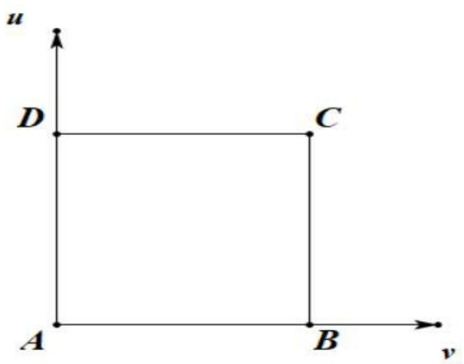

Figure 3. The pixel coordinate system.

Putting the fours coordinate systems together, we could obtain the diagram shown in Figure 4.

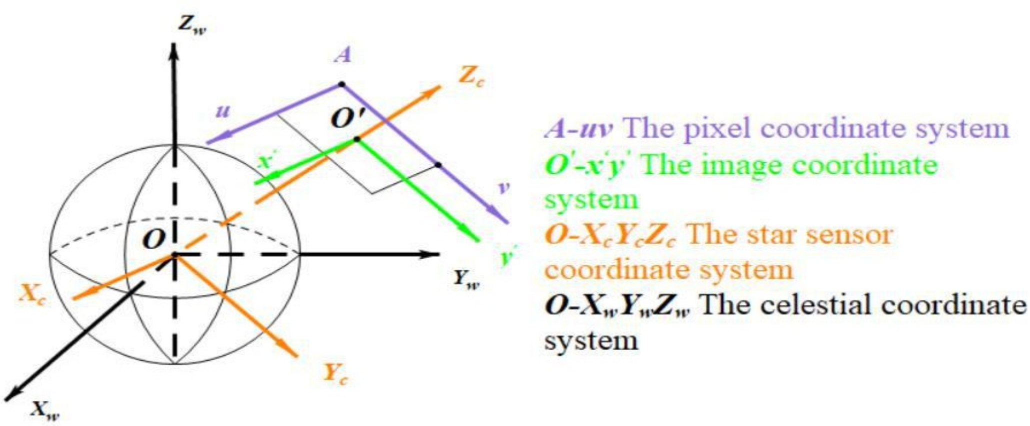

Figure 4. Four coordinate systems (Please refer to Table 1 for the definition of notations).

2.2. Notations

Table 1. The definition of notations.

Meaning	Notation	Description
	D	The intersection points of the celestial sphere and the optical axis
	O	The projection center
POINT	O'	The projection points of the point O on the photosensitive surface
	Pi	The i^{th} star, where the index i is greater than 0
	Qi	The projection points of the i^{th} star P_i on the photosensitive surface, where the index i is greater than 0
	∂	The right ascension
	δ	The declination
VARIABLE	f	The distance between the point O and the point O' on the photosensitive surface
	r	The distance between the point O and the point Q_i on the photosensitive surface
	(x_0, y_0, z_0)	The coordinate of the point □ in the star sensor coordinate system
	(x_i, y_i, z_i)	The coordinate of the star P_i in the star sensor coordinate system
COORDINATE	$(r_0, \alpha_0, \delta_0)$	The coordinate of projection points O' in the star sensor coordinate system
	$(r_i, \alpha_i, \delta_i)$	The coordinate of projection points Q_i in the star sensor coordinate system
	(x_i, y_i)	The coordinate of the point Q_i in the image coordinate system
	(u_i, v_i)	The coordinate of the point Q_i in the pixel coordinate system

2.3. Establishment of Coordinate Systems

To simplify the problem, we make some reasonable assumptions.

● The vernal equinox does not shift. While the vernal equinox keeps moving westward, the impact on time is quite slow and small (The tropical year is reduced by 0.5s per century), so that the shift can be ignored.

● The centroid positioning deviation of the star can be ignored. The distance between a star and the projection center can be regarded as infinite, so that a star can be seen as an ideal particle.

● The radius of the celestial sphere is large enough. The definition of the celestial sphere, the radius is infinite.

● The projection center is the center of the celestial sphere. Since the definition of the celestial sphere has infinite radius, the distance from the center of the earth to the projection center is so small that can be ignored.

● The optical center of the lens is the center of the earth. Because the optical center of the lens is the projection center, based on the last assumption, it can be considered as the center of the earth.

● All stars are on the celestial sphere. Because the radius of the celestial sphere is quite large, the distances from the projection center to different stars can be regarded as the same.

3. Model Overview

To determine the coordinate of the point D, we establish a model to illustrate the geometrical relationship. If the distance f *between* the point O to the point O' is unknown, the calculation may be complex, we use

Newton's method to simplify it.

Once we get the coordinate of the point D , we are required to find a principle to select proper stars for improving the accuracy. There are two influence factors, namely the number of stars and the geometrical positions of stars. We will firstly establish a model to screen which stars in Annex 1 may be captured by the star sensor. Then we transform the coordinates in the celestial coordinate system into the pixel coordinate system to conduct further screening. Since the principle should be effective no matter where the photosensitive surface is, we discuss the situation when the optical axis points to the north celestial pole.

4. Model Development

4.1. Coordinates of the Intersection Point D

4.1.1. Establishment of the Tetrahedral Model

Given the position of three stars (P_1, P_2, P_3) and their projection (Q_1, Q_2, Q_3) on the photosensitive surface, we connect projections and the center O and get a tetrahedral model shown in Figure 5. To simplify the problem, we establish a spherical coordinate system based on the celestial coordinate system.

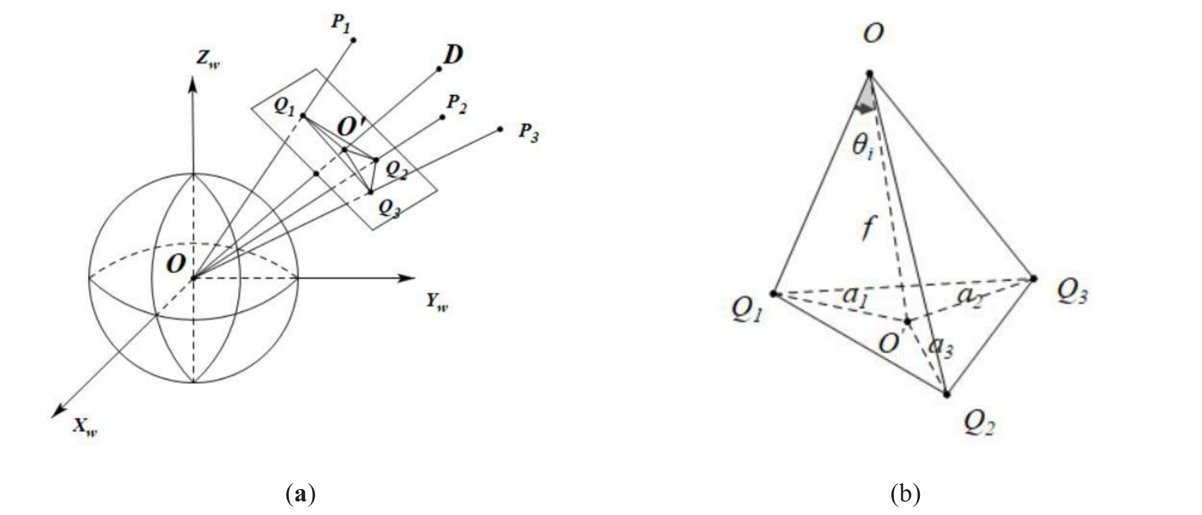

Figure 5. The tetrahedral model.

In the spherical coordinate system, we interpret r_i as the distance of one point in the photosensitive surface to the center of the celestial sphere O, and the index i indicates the i^{th} star. Then we get coordinates $Q_i(r_i, \delta_i, \alpha_i)$ and $O'(f, \delta_0, \alpha_0)$. Then we could calculate the cosine of the angle between half–line OQ_i and OO' according to the formular

$$\cos\left\langle \overrightarrow{OQ_i}, \overrightarrow{OO'} \right\rangle = \cos\theta_i = \cos\delta_i \cos\delta_0 \cos(\alpha_0 - \alpha_i) + \sin\delta_i \sin\delta_0 \tag{1}$$

We cut the tetrahedron by crossing $\Delta OQ_1O'$ and show the profile in Figure 6.

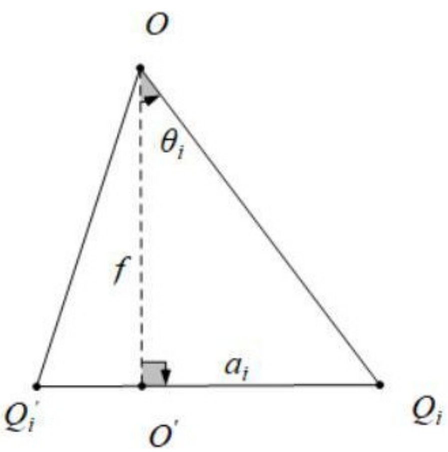

Figure 6. The profile.

According to properties of triangles, the cosine of the angle θ_i between half–line OQ_i and half–line OO' can be expressed as

$$\cos\theta_{\mathrm{i}} = \frac{f}{\sqrt{\alpha_i^2 + f^2}} \tag{2}$$

With equation (1), equation (2) and coordinates of $O, Q_1, Q_2\, and\, Q_3$, we could obtain an equation set

$$\begin{cases} \cos\delta_1 \cos\delta_0 \cos(\alpha_0 - \alpha_1) + \sin\delta_1 \sin\delta_0 = \dfrac{f}{\sqrt{\alpha_1^2 + f^2}} \\ \cos\delta_2 \cos\delta_0 \cos(\alpha_0 - \alpha_2) + \sin\delta_2 \sin\delta_0 = \dfrac{f}{\sqrt{\alpha_2^2 + f^2}} \\ \cos\delta_3 \cos\delta_0 \cos(\alpha_0 - \alpha_3) + \sin\delta_3 \sin\delta_0 = \dfrac{f}{\sqrt{\alpha_3^2 + f^2}} \end{cases} \tag{3}$$

With coordinates of $, Q_1, Q_2\, and\, Q_3$, we could get three equations with variables f, α_0 and δ_0. If the variable f is already known, with MATLAB, we obtain the value of α_0 and δ_0 to represent the location of D.

4.1.2. Solution of the Model with Newton's Method

If the variable ƒ is unknown, the equation set (3) is difficult to compute directly, so that we iteratively approximate the solution of the non–linear equation set using Newton's method.

Set the equation set (3) as

$$\begin{cases} f_1(f, \quad \alpha_0, \quad \delta_0) = 0 \\ f_2(f, \quad \alpha_0, \quad \delta_0) = 0 \\ f_3(f, \quad \alpha_0, \quad \delta_0) = 0 \end{cases} \tag{3}$$

Where $$f_i(f, \quad \alpha_0, \quad \delta_0) = \cos\delta_i \cos\delta_0 \cos(\alpha_0 - \alpha_i) + \sin\delta_i \sin\delta_0 - \frac{f}{\sqrt{\alpha_i^2 + f^2}} \tag{4}$$

The solution set and the equation set can be expressed as vectors $x = (f \quad \alpha_0 \quad \delta_0)^T$ and $F = (f_1 \quad f_2 \quad f_3)^T$ respectively, so that the equation set (4) can be expressed as

$$F(x) = 0 \tag{5}$$

After getting an approximate solution $x^{(k)} = (f^{(k)} \quad \alpha_0^{(k)} \quad \delta_0^{(k)})^T$, we expand components $f_i(x)$ of the function F(x) by Taylor formula and obtain

$$F(x) \approx \mathrm{F}(\mathrm{x}^{(k)}) + \mathrm{F}^{'}(x^{(k)})(x - x^{(k)}) \tag{6}$$

Substituting equation (6) into (5)a, a linear equation set could be attained

$$F'(x^{(k)})(x - x^{(k)}) = -F(x^{(k)}) \tag{7}$$

Where,

$$F^{'}(x) = \begin{bmatrix} \dfrac{\partial f_1(x)}{\partial f} & \dfrac{\partial f_1(x)}{\partial \alpha_0} & \dfrac{\partial f_1(x)}{\partial \beta_0} \\ \dfrac{\partial f_2(x)}{\partial f} & \dfrac{\partial f_2(x)}{\partial \alpha_0} & \dfrac{\partial f_2(x)}{\partial \beta_0} \\ \dfrac{\partial f_3(x)}{\partial f} & \dfrac{\partial f_3(x)}{\partial \alpha_0} & \dfrac{\partial f_3(x)}{\partial \beta_0} \end{bmatrix}$$

Here $F'(x)$ is the Jacobi matrix of $F(x)$. Solving the equation set (7), we get the solution vector

$$x^{(k+1)} = x^{(k)} - F'(x^{(k)})^{-1} + F(x^{(k)})$$

4.2. Selection Principle of Stars

4.2.1. Projection Screening Model

Before discussing how to improve the accuracy of the intersection point D, we establish a model to determine the number of stars on the photosensitive surface. As it mentioned above, the field of view of the star sensor is $12^{\circ} \times 12^{\circ}$, and the pixel is 512×512, so we set the length of its side is d. Although the star sensor may rotate around the celestial sphere center O, rotations around X_w axis, Z_w axis or Y_w axis are similar. Hence, we ignore the rotation. We get the circle $\odot O'$ as the externally tangent circle of the square. The radius of the circle □ O' is $\frac{d}{\sqrt{2}}$. We sketch the model in Figure 7.

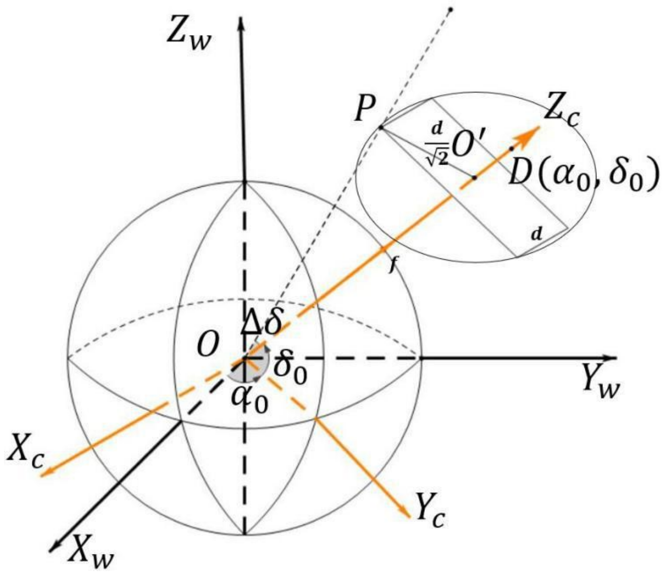

Figure 7. The projection screening model.

As it shown in the graph, the point P_i can be exactly observed by the star sensor, and the angle $\Delta\delta$ the angle between the line OP and the line OO'. In the triangle $\Delta OO'P$, the lengths of the line segment $O'D$ and the line segment OO' are $\frac{d}{\sqrt{2}}$ and f respectively. According to the properties of triangle, we could get

$$\Delta\delta = \tan^{-1}(\frac{d}{\sqrt{2}f})$$

Using the same way, we could get

$$\Delta\alpha = \tan^{-1}(\frac{d}{\sqrt{2}f\cos\delta_0})$$

Therefore, domains of the declination and the right ascension can be written as

$$\begin{cases} \alpha \in [\alpha_0 - \Delta\alpha, \quad \alpha_0 + \Delta\alpha] \\ \delta \in [\delta_0 - \Delta\delta, \quad \delta_0 + \Delta\delta] \end{cases}$$

With Annex 1, if the location of the star sensor is known, we could determine which stars can be projected on the externally tangent circle of the photosensitive surface. Then, we transform coordinates to determine whether the star P_i can project on the photosensitive surface.

4.2.2. Transformation of Coordinate Systems

In order to improve the accuracy of point D, we are required to select proper stars according to the geometric position. For ease of calculation, we need to transfer coordinates from the celestial coordinate system to the pixel coordinate system. Since there are four coordinate systems, after implementing the pairwise transformation, we can obtain a final transformation formula.

Both the celestial coordinate system and the star sensor coordinate system are three−dimensional. With the assumption that the projection center is the center of the celestial sphere, their origins are overlapped. Thus, the transformation process can be seen as the point rotate φ, ϖ and β about X_w axis, Y_w axis and Z_w axis respectively. For the rotation around Z_w axis, the transformation is

$$\begin{cases} x = x' \\ y = y'\cos\varphi + z'\cos\varphi \\ z = -y'\sin\varphi + z'\cos\varphi \end{cases}$$

Where x, y and z indicate the transformed coordinates, and x', y' and z' represent the original coordinates. The equation set can be written as

$$\begin{bmatrix} x \\ y \\ z \end{bmatrix} = \begin{bmatrix} \cos\beta & -\sin\beta & 0 \\ \sin\beta & \cos\beta & 0 \\ 0 & 0 & 1 \end{bmatrix} \begin{bmatrix} x' \\ y' \\ z' \end{bmatrix} = R_z \begin{bmatrix} x' \\ y' \\ z' \end{bmatrix}$$

Using the same way, the transformations about X_w axis and Y_w axis are

$$\begin{bmatrix} x \\ y \\ z \end{bmatrix} = \begin{bmatrix} 1 & 0 & 0 \\ 0 & \cos\varphi & \sin\varphi \\ 0 & -\sin\varphi & \cos\varphi \end{bmatrix} \begin{bmatrix} x' \\ y' \\ z' \end{bmatrix} = R_x \begin{bmatrix} x' \\ y' \\ z' \end{bmatrix}$$

$$\begin{bmatrix} x \\ y \\ z \end{bmatrix} = \begin{bmatrix} \cos\varpi & 0 & \sin\varpi \\ 0 & 1 & 0 \\ -\sin\varpi & 0 & \cos\varpi \end{bmatrix} \begin{bmatrix} x' \\ y' \\ z' \end{bmatrix} = R_y \begin{bmatrix} x' \\ y' \\ z' \end{bmatrix}$$

Set the matrix $R = R_x R_y R_z$, the transformation formula from the celestial coordinate system to the star sensor coordinate is

$$\begin{bmatrix} X_c \\ Y_c \\ Z_c \end{bmatrix} = R^{-1} \begin{bmatrix} X_w \\ Y_w \\ Z_w \end{bmatrix} \tag{8}$$

Here R^{-1} is the inverse matric of the matrix R

Then we need to transform the coordinate into the image coordinate system. Putting the celestial coordinate system and the image coordinate system together, we sketch the graph in Figure 8.

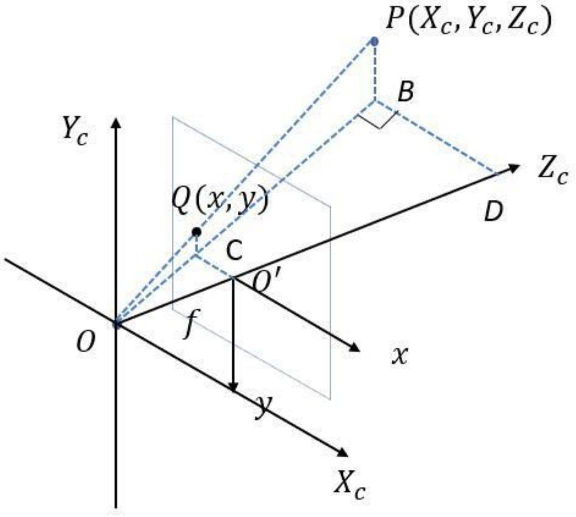

Figure 8. The celestial coordinate system and the image coordinate system.

In the graph, the photosensitive surface, the plane POB and the plane X_cOZ_c are perpendicular to each other and intersects at line BO , line QC and line $O'C$. Therefore, it indicates that ΔDBO is similar to $\Delta O'CO$. and ΔPBO is similar to ΔQCO . According to the properties of similar triangles

$$\frac{DB}{OC} = \frac{DO}{O'O} = \frac{PB}{QC} = \frac{X_c}{x} = \frac{Z_c}{f} = \frac{Y_c}{y}$$

We get
$$\begin{cases} x = f\dfrac{X_c}{Z_c} \\ y = f\dfrac{X_c}{Y_c} \end{cases}$$

Thus, the transformation formula from the star sensor coordinate to the image coordinate system is

$$Z_c\begin{bmatrix} x \\ y \\ 1 \end{bmatrix} = \begin{bmatrix} f & 0 & 0 \\ 0 & f & 0 \\ 0 & 0 & f \end{bmatrix}\begin{bmatrix} X_c \\ Y_c \\ Z_c \end{bmatrix}$$

Finally, for ease of calculation, we transform coordinates from the image coordinate system to the pixel coordinate system. We put two systems together again to get the diagram in Figure 9.

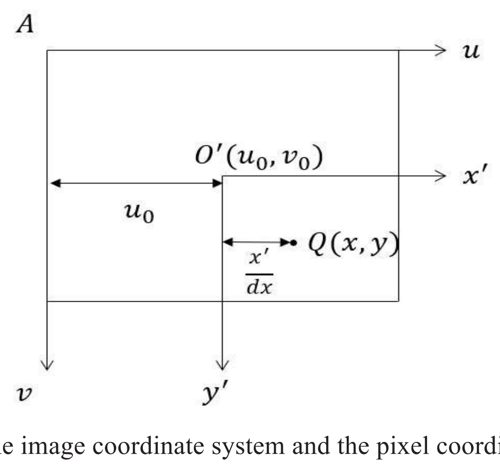

Figure 9. The image coordinate system and the pixel coordinate system.

Since the unit in two systems are different, following equation set helps us to unify units.

$$\begin{cases} u = \dfrac{x}{dx} + u_o \\ v = \dfrac{y}{dy} + v_o \end{cases}$$

And it can be written as

$$\begin{bmatrix} u \\ v \\ 1 \end{bmatrix} = \begin{bmatrix} \dfrac{1}{dx} & 0 & u_o \\ 0 & \dfrac{1}{dy} & v_o \\ 0 & 0 & 1 \end{bmatrix} \begin{bmatrix} x \\ y \\ 1 \end{bmatrix} \tag{10}$$

Meanwhile, it is the transformation formula. Combining equations (8), (9) and (10), we deduce the ultimate transformation formula from the celestial coordinate system to the pixel coordinate system.

$$Z_c \begin{bmatrix} u \\ v \\ 1 \end{bmatrix} = \begin{bmatrix} \dfrac{1}{dx} & 0 & u_0 \\ 0 & \dfrac{1}{dy} & v_0 \\ 0 & 0 & 1 \end{bmatrix} \begin{bmatrix} f & 0 & 0 \\ 0 & f & 0 \\ 0 & 0 & 1 \end{bmatrix} R^{-1} \begin{bmatrix} X_w \\ Y_w \\ Z_w \end{bmatrix} \tag{11}$$

4.2.3. The Selection Principle

After operating the above two steps, we could get the ultimate star map for a specific location of the star sensor. In the star map, we get the number N of stars and coordinates of stars in the pixel coordinate system. Since it is better to avoid selecting stars at the edge of the photosensitive surface, we take the average distance □ of the distances a_i between the point Q_i and the point O' as the criteria, i.e., $a = \frac{1}{3}\sum_{i=1}^{3} a_i$. In addition, because our main aim is to determine a selection principle for improving accuracy of the point D, we only consider the situation that the optical Z_c points to the north celestial pole. Under this situation, considering the right ascension α_0 of the point D is meaningless and the declination δ_0 of the point D is 90°. Hence, we only need to compare the calculation values with the true declination 90°. Although the number of stars in Annex 1 is quite large, the number N of stars of a specific star map is countable. Therefore, if we select three stars each time, then we need to try C_N^3 times.

For each try, we calculate the coordinate of the point D by our tetrahedral model and define declination values of these coordinates as δ_j (for $j = 1, 2, ..., C_N^3$). Therefore, we attain a graph plotting declination values δ_j versus the average distance a. We conclude that the accuracy of the point D improves as the average distance a is declining.

For there are only three stars for each try, we get the principle shown in Figure 10

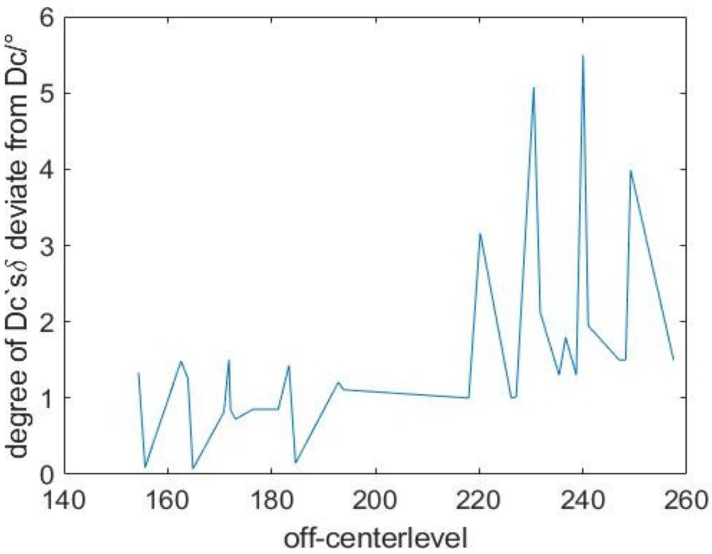

Figure 10. The principle when we select only three stars.

If we choose only three stars to determine the coordinate of the point D, they could compose a triangle or a line segment. However, if the number of stars is n, which is greater than 3, then the geometric positions may be complex. In this situation, for a point set, we choose three of them to calculate the coordinate of the point D, so that we should try C_n^3 times for each point set. We still indicate a as the average distance between the point Q_i and the point O. We firstly compute the average value of declination δ_j, i.e., $\bar{\delta} = \frac{1}{n}\sum_{j=1}^{n}\delta_j$, and define the deviation is $\varepsilon = \bar{\delta} - \delta_0$. We define a vector p to represent the performance of different sets on accuracy.

$$p = \begin{bmatrix} C_n^3 & a & \varepsilon \end{bmatrix}^T$$

With MATLAB, we plot vector *p* in Figure 11.

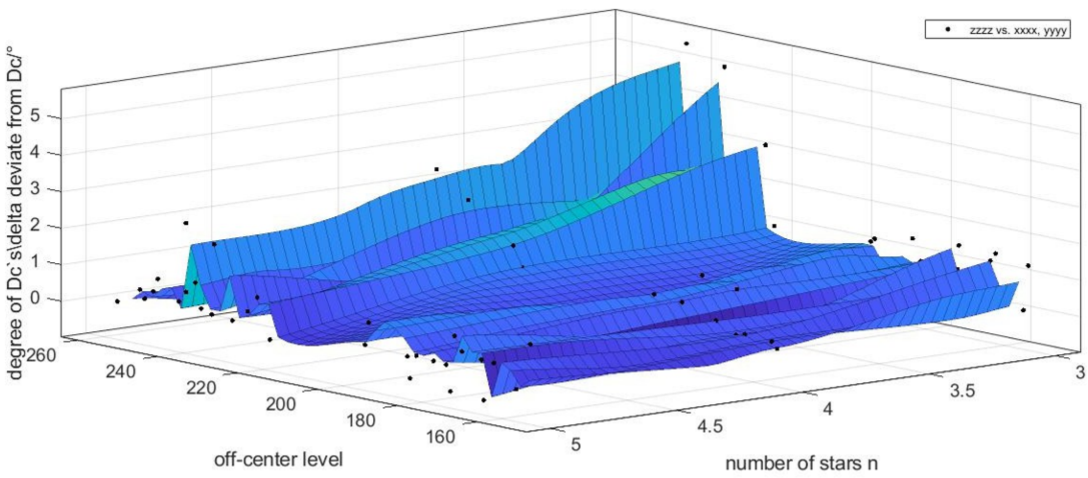

According to the graph, we conclude that the accuracy improves as the average distance falls.

4.3. The Matching Recognition Model

4.3.1. The Feature Database Model for Navigation Stars Based on Triangles

Before achieving matching recognition, we should extract feature as criteria. For a navigation star P_i in Annex 1, we could sketch its position. Based on the assumption that all stars are on the celestial sphere, and because they are close to each other, we could invert their given coordinate (α_i, δ_i) into (x_i, y_i, z_i) and find its nearest three navigation stars P_{i+1}, P_{i+2} and P_{i+3} in Figure 12.

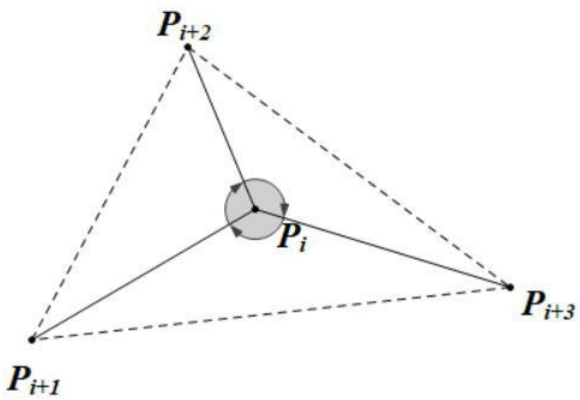

Figure 12. The navigation star P_i and its closest three stars.

The algorithm is shown as follow:

INPUT: (α_i, δ_i) for $i = 1, 2, ...N_w$ the coordinate of all navigation stars, where N_w indicate the total number of navigation stars.

PROCESS:

STEP 1: Based on the transformation formula (8), find the closest navigation stars P_{i+1}, P_{i+2} and P_{i+3} of the navigation star P_i.

STEP 2: Calculate angles $\angle P_{i+1}P_iP_{i+2}, \angle P_{i+2}P_iP_{i+3}$ and $\angle P_{i+1}P_iP_{i+3}$.

STEP 3: Record angles from small to large as the feature vector for the navigation star P_i

STEP 4: Repeat STEP 1 to STEP 3 till i equal to N_w

OUTPUT: The feature database matrix K_w, for which the columns are feature vectors k_w

4.3.2. The Feature Database Model for Star Maps Based on Triangles

We interpret N_c as the number of stars for a specific star map. Using the same algorithm, we could extract the feature vector. However, based on our selection principle, we should ignore stars on the edge of the star map to decline the deviation. There will be n_c feature vectors, where n_c is less than N_c. Therefore, the algorithm is:

INPUT: (α_i, δ_i) for $i = 1, 2, ...N_c$ the coordinate of all navigation stars

PROCESS:

STEP 1: Based on the transformation formula (8), find the closest navigation stars P_{i+1}, P_{i+2} and P_{i+3} of the navigation star P_i.

STEP 2: Calculate angles $\angle P_{i+1}P_iP_{i+2}, \angle P_{i+2}P_iP_{i+3}$ and $\angle P_{i+1}P_iP_{i+3}$.

STEP 3: Record angles from small to large as the feature vector for the navigation star P_i.

STEP 4: Repeat STEP 1 to STEP 3 till i equal to n_c.

OUTPUT: The feature database matrix K_c, for which the columns are feature vectors k_c.

4.3.3. The Matching Recognition Algorithm

After extracting features matrix K_w and K_c, we employ the matching recognition algorithm to find the corresponding number of stars in Annex 2. The algorithm is shown below:

INPUT: Features matrix K_w and K_c, the error ε'

PROCESS:

STEP 1: Compare the feature matrix K_c of star maps with that of navigation stars and record the navigation stars which satisfy $\|K_c - K\| \le \varepsilon'$ as set M.

STEP 2: Cluster stars in the set M by DBScan algorithm.

STEP 3: Compare the center of clustering to determine the best navigation stars.

STEP 4: Repeat STEP 1 to STEP 3 till all navigation stars have been considered.

OUTPUT: The corresponding number for star maps in Annex 2.

4.3.4. Results

With above three algorithms, we could get the number of navigation stars. Take the second star map in Annex 2 as example, we get the star map in Figure 13 and the star table in Table 2

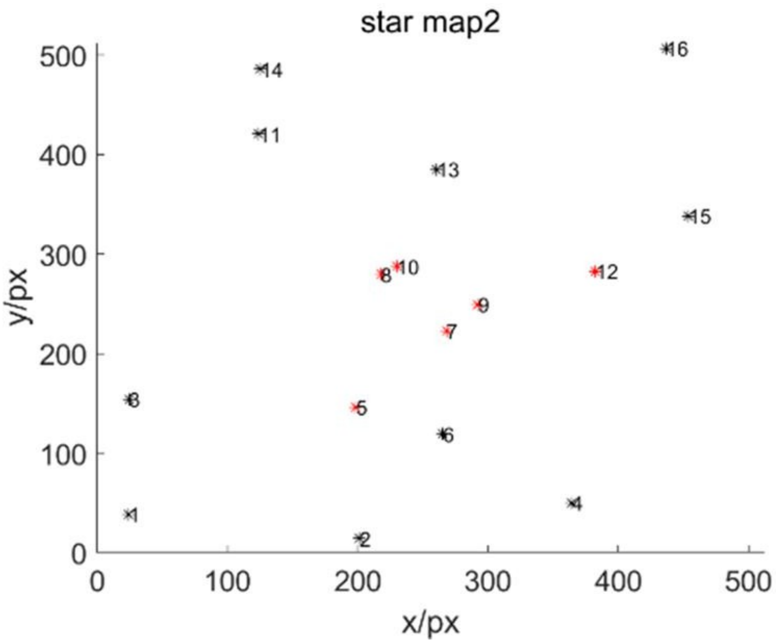

Figure 13. Star map 2.

Table 2. The star table for star map 2.

Number	Right Ascension	Declination	Number of Navigation stars
B01	24.23	38.41	518
B02	201.29	14.37	472
B03	24.39	154.16	537
B04	364.31	50.23	428
B05	198.44	145.88	491
B06	265.22	119.01	469
B07	268.41	222.59	482
B08	217.73	279.38	503
B09	292.36	249.03	478
B10	229.82	287.51	499
B11	123.64	420.49	547
B12	382.53	282.53	460

Cont.

Number	Right Ascension	Declination	Number of Navigation stars
B13	260.42	384.87	507
B14	125.27	485.79	556
B15	453.94	338.11	447
B16	436.79	506.43	479

The marked points namely, 5 ,7, 8,9,10,12 are navigation stars. We attach full answer in Appendix, namely, four–star maps and their corresponding navigation stars.

5. Strength and Weakness

5.1. Strength

● Our model is based on reasonable assumptions. That is to say, the positioning problem for the point D is transformed into a geometric problem according to mechanism analysis.

● Based on the coordinate transformation formula, our model converts coordinates from the celestial coordinate system into the pixel coordinate system.

● Considering the accuracy of the point D, we establish a rational model to screen points of the star map for a specific time.

● When considering the influence factors of accuracy, we simplify the question and emphasize the main point by taking the north celestial pole as an example.

5.2. Weakness

● When we consider the transformation from the celestial coordinate system into the star sensor coordinate system, only the situation that the optical axis rotates around X_c axis is taken into account. We do not consider the rotation of the optical axis around Y_c axis and Z_c axis.

● In our first model for the coordinate of the point D, we use the Newton's method. However, errors are generated during the iterative process. Apart from this, we can only get the numerical solution instead of the analytic solution.

● We ignore that the projection of stars centroid may be biased.

6. Conclusion

Through the establishment of three models, we achieve feature extraction and matching recognition of star sensors. First, we establish a geometrical model to convert the coordinate question into the algebraic question. Then we employ Newton's method to simplify the question.

Then, in order to draw a principle for improving accuracy, we consider the star map at the north celestial pole as an example. For different number and geometrical position of stars, we compare the deviation between the calculated value and the true value. Hence, we draw the conclusion that on the photosensitive surface, if selected stars are closer to the center, then the accuracy is relatively better.

After determining the principles, we extract the feature vectors of the given star tables and the star map. We use the DBScan clustering algorithm to implement the matching recognition process. Ultimately, we get the results of star map and numbers for navigation stars.

Funding

Not applicable.

Author Contributions

Conceptualization, M.W. and H.Z.; writ-ing—original draft preparation and writing—review and editing, M.W., H.Z. and N.Z. All authors have read and agreed to the published version of the manuscript.

Institutional Review Board Statement

Not applicable.

Informed Consent Statement

Not applicable.

Data Availability Statement

Not applicable.

Conflicts of Interest

The authors declare no conflict of interest.

Reference

1 Kundu S, Fu Y, Ye B, Beerel P. A, Pedram M. Toward Adversary-aware Non-iterative Model Pruning through Dynamic Network Rewiring of DNNs. *ACM Transactions on Embedded Computing Systems* 2022; **21**(**5**): 1–24.

2 Li S, Dong X, Ma D, Dang B, Zang H, Gong Y. Utilizing the LightGBM Algorithm for Operator User Credit Assessment Research. 2024. DOI: 10.48550/arXiv.2403.14483.

3 Liu T, Xu C, Qiao Y, Jiang C, Chen W. News Recommendation with Attention Mechanism. 2024. DOI: 10. 48550/arXiv.2402.07422.

4 Ju Y, Lam K–M, Xie W, Zhou H, Dong J, Shi B. Deep Learning Methods for Calibrated Photometric Stereo and Beyond: A Survey. 2022. DOI: 10.48550/arXiv.2212.08414.

5 Ju Y, Shi B, Chen Y, Zhou H, Dong J, Lam K–M. GR–PSN: Learning to Estimate Surface Normal and Reconstruct Photometric Stereo Images. *IEEE Transactions on Visualization and Computer Graphics* 2023; 1–16. DOI: 10.1109/TVCG.2023.3329817.

6 Wang X, Xiao T, Tan J, Ouyang D, Shao J. MRMRP: Multi–Source Review–Based Model for Rating Prediction. In Proceedings of the Database Systems for Advanced Applications: 25th International Conference, DASFAA 2020, Jeju, South Korea, 24–27 September 202.

7 Wang X, Xiao T, Shao J. Emrm: Enhanced Multi–Source Review–Based Model for Rating Prediction. In Proceedings of the Knowledge Science, Engineering and Management: 14th International Conference, KSEM 2021, Tokyo, Japan, 14–16 August 2021.

8 Hu J, Wang X, Liao Z, Xiao T. M–Gcn: Multi–Scale Graph Convolutional Network for 3d Point Cloud Classification. In Proceedings of the 2023 IEEE International Conference on Multimedia and Expo (ICME), Brisbane, Australia, 10–14 July 2023.

9 Xia D, Alexander AK, Isbell A, Zhang S, Ou J, Liu XM. Establishing a Co–Culture System for Clostridium Cellulovorans and Clostridium Aceticum for High Efficiency Biomass Transformation. *J Sci Heal Univ Ala* 2017; **14**: 8–13.

10 Li S, Kou P, Ma M, Yang H, Huang S, Yang Z. Application of Semi–supervised Learning in Image Classification: Research on Fusion of Labeled and Unlabeled Data. *IEEE Access* 2024; **12**: 27331–27343.

11 Wu Y, Jin Z, Shi C, Liang P, Zhan T. Research on the Application of Deep Learning–based BERT Model in Sentiment Analysis. 2024. DOI: 10.48550/arXiv.2403.08217.

12 Dai W. Safety Evaluation of Traffic System with Historical Data Based on Markov Process and Deep–Reinforcement Learning. *Journal of Computational Methods in Engineering Applications* 2021; **1**(**1**): 1–14.

13 Yu F, Milord JO, Flores LY, Marra R. Work in Progress: Faculty Choice and Reflection on Teaching

Strategies to Improve Engineering Self–Efficacy. In Proceedings of the 2022 ASEE Annual Conference, Minneapolis, MN, USA, 26–29 June 2022.

14 Li S, Singh K, Riedel N, Yu F, Jahnke I. Digital Learning Experience Design and Research of a Self–Paced Online Course for Risk–Based Inspection of Food Imports. *Food Control* 2022; **135**: 108698.

15 Hao Y, Chen Z, Jin J, Sun X. Joint Operation Planning of Drivers and Trucks for Semi–Autonomous Truck Platooning. *Transportmetrica A: Transport Science* 2023; 1–37. DOI: 10.1080/23249935.2023.2266041.

16 Hao Y, Chen Z, Sun X, Tong L. Planning of Truck Platooning for Road–Network Capacitated Vehicle Routing Problem. 2024; DOI: 10.48550/arXiv.2404.13512.

17 Deng X, Li L, Enomoto M, Kawano Y. Continuously Frequency–Tuneable Plasmonic Structures for Terahertz Bio–Sensing and Spectroscopy. *Scientific reports* 2019; **9**(**1**): 3498.

18 Sugaya T, Deng X, Kawano Y. Resonant Frequency Tuning of Terahertz Plasmonic Structures Based on Solid Immersion Method. In Proceedings of the 2019 44th International Conference on Infrared, Millimeter, and Terahertz Waves (IRMMW–THz), Paris, France, 1–6 September 2019.

19 Lu Y, Wang Y, Parikh D, Xin Y, Lu G. Extending Single Beam Lidar to Full Resolution by Fusing with Single Image Depth Estimation. In Proceedings of the 2020 25th International Conference on Pattern Recognition (ICPR), 10–15 January 2021, Milan, Italy.

20 Lu Y, Zhang J, Sun S, Guo Q, Cao Z, Fei S, Yang B, Yingjie Chen. Label–Efficient Video Object Segmentation with Motion Clues. *IEEE Transactions on Circuits and Systems for Video Technology* 2023. DOI: 10.1109/TCSVT.2023.3298853.

21 Lu Y, Wang Y, Parikh D, Khan A, Lu G. Simultaneous Direct Depth Estimation and Synthesis Stereo for Single Image Plant Root Reconstruction. *IEEE Transactions on Image Processing* 2021; **30**: 4883–4893.

22 Ju Y, Jian M, Wang C, Zhang C, Dong J, Lam K–M. Estimating High–Resolution Surface Normals Via Low –Resolution Photometric Stereo Images. *IEEE Transactions on Circuits and Systems for Video Technology*, 2023; **34**(**4**): 2512–2524.

23 Song X, Wu D, Zhang B, Peng Z, Dang B, Pan F, Wu Z. Zeroprompt: Streaming Acoustic Encoders Are Zero–Shot Masked LMs. 2023; DOI: 10.48550/arXiv.2305.10649.

24 Yao J. Ndc–Scene: Boost Monocular 3d Semantic Scene Completion in Normalized Device Coordinates Space. In Proceedings of the 2023 IEEE/CVF International Conference on Computer Vision (ICCV), Paris, France, 1–6 October 2023.

25 Yao J, Wu T, Zhang X. Improving Depth Gradient Continuity in Transformers: A Comparative Study on Monocular Depth Estimation with CNN. 2023. DOI: 10.48550/arXiv.2308.08333.

26 Yao J, Pan X, Wu T, Zhang X. Building Lane–Level Maps from Aerial Images. In Proceedings of the ICASSP 2024–2024 IEEE International Conference on Acoustics, Speech and Signal Processing (ICASSP), Seoul, Korea, 14–19 April 2024.

27 Cheng S, Chu B, Zhong B, Zhang Z, Liu X, Tang ZJ, Li XX. DRNet: Towards Fast, Accurate and Practical Dish Recognition. *Science China Technological Sciences* 2021; **64**(**12**): 2651–2661.

28 Guo Q, Yu Z, Fu J, Lu Y, Zweiri Y, Gan D. Force–EvT: A Closer Look at Robotic Gripper Force Measurement with Event–based Vision Transformer. 2024. DOI: 10.48550/arXiv.2404.01170.

29 Li Z, Huang Y, Zhu M, Zhang J, Chang J, Liu H. Feature Manipulation for DDPM Based Change Detection. 2024. DOI: 10.48550/arXiv.2403.15943.

30 Li S, Qu H, Dong X, Dang B, Zang H, Gong Y. Leveraging Deep Learning and Xception Architecture for High–Accuracy MRI Classification in Alzheimer Diagnosis. 2024. DOI: 10.48550/arXiv.2403.16212.

31 Zeng L, Li H, Xiao T, Shen F, Zhong Z. Graph Convolutional Network with Sample and Feature Weights for Alzheimer'S Disease Diagnosis. *Information Processing & Management* 2022; **59**(**4**): 102952.

32 Xiao T, Zeng L, Shi X, Zhu X, Wu G. Dual–Graph Learning Convolutional Networks for Interpretable Alzheimer'S Disease Diagnosis. In Proceedings of the International Conference on Medical Image *Computing and Computer–Assisted Intervention* 18–22 September 2022, Singapore.

33 Sun G, Zhan T, Owusu BG, Daniel A–M, Liu G, Jiang W. Relational Reinforcement Learning Based Autonomous Cell Activation in Cloud-RANs. *Future Generation Computer Systems* 2020; **104**: 60–73.

34 Dai W, Jiang Y, Mou C, Zhang C. An Integrative Paradigm for Enhanced Stroke Prediction: Synergizing Xgboost and Xdeepfm Algorithms. In Proceedings of the Proceedings of the 2023 6th International Conference on Big Data Technologies, Qingdao, China, 22–24 September 2023.

35 D Ma, S Li, B Dang, H Zang, X Dong. Fostc3net: A Lightweight YOLOv5 Based On the Network Structure Optimization. 2024. DOI: 10.48550/arXiv.2403.13703.

36 Dai W, Mou C, Wu J, Ye X. Diabetic Retinopathy Detection with Enhanced Vision Transformers: The Twins –Pcpvt Solution. In Proceedings of the 2023 IEEE 3rd International Conference on Electronic Technology, Communication and Information (ICETCI), Changchun, China, 26–28 May 2023.

37 Liu T, Xu C, Qiao Y, Jiang C, Yu J. Particle Filter SLAM for Vehicle Localization. 2024. DOI: 10.48550/arXiv.2402.07429.

38 Zhou H, Lan T, Aggarwal V. Pac: Assisted Value Factorization with Counterfactual Predictions in Multi – Agent Reinforcement Learning. Advances in Neural Information Processing Systems 2022; **35**: 15757 – 15769.

39 Mei Y, Zhou H, Lan T, Venkataramani G, Wei P. MAC-PO: Multi-Agent Experience Replay via Collective Priority Optimization. 2023. DOI: 10.48550/arXiv.2302.10418.

40 Zhou H, Lan T, Aggarwal V. Value Functions Factorization with Latent State Information Sharing in Decentralized Multi – Agent Policy Gradients. *IEEE Transactions on Emerging Topics in Computational Intelligence* 2023; **7**(**5**): 1351–1361.

41 Zhang Z, Zhong B, Zhang S, Tang Z, Liu X, Zhang Z. Distractor – Aware Fast Tracking Via Dynamic Convolutions and Mot Philosophy. In Proceedings of the Proceedings of the 2021 IEEE/CVF Conference on Computer Vision and Pattern Recognition, Nashville, TN, USA, 20–25 June 2021.

42 Deng X, Dong Z, Ma X, Wu H, Wang B, Du X. Exploration on Mechanics Design for Scanning Tunneling Microscope. In Proceedings of the 2009 Symposium on Photonics and Optoelectronics, Wuhan, China, 14–16 August 2009.

43 Deng X, Simanullang M, Kawano Y. Ge-Core/a-Si-Shell Nanowire-Based Field-Effect Transistor for Sensitive Terahertz Detection. *Photonics* 2018; **5**(**2**): 13.

44 Su J, Jiang C, Jin X, Qiao Y, Xiao T, Ma H, Wei R, Jing Z, Xu J, Lin J. Large Language Models for Forecasting and Anomaly Detection: A Systematic Literature Review. 2024. 10.48550/arXiv.2402.10350.

45 Schubert E, Sander J, Ester M, Kriegel HP, Xu X. DBSCAN Revisited, Revisited: Why and How You Should (Still) Use DBSCAN. *ACM Transactions on Database Systems (TODS)* 2017; **42**(**3**): 1–21.